Heliyon 10 (2024) e33139

Contents lists available at ScienceDirect

Heliyon

journal homepage: www.cell.com/heliyon

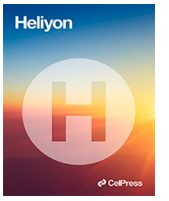

Research article

[Nd(NTA)2·H_2O]$^{3-}$ complex with high-efficiency emission in NIR region

M. Sasani Ghamsari [a,*], M.M. Arghavan [b]

[a] Photonics and Quantum Technologies Research School, Nuclear Science and Technology Research Institute, 11155-3436, Tehran, Iran
[b] Department of Physics, Payame Noor University, P.O.Box 19395-3697, Tehran, Iran

ARTICLE INFO

Keywords:
Nd(NTA)2
$H_2O]^{3-}$ complex
Full-width at half maximum (FWHM)
Judd-Ofelt theory
NIR emission
Bioimaging

ABSTRACT

The distinctive photophysical characteristics possessed by lanthanides, including europium, neodymium, and ytterbium, render them adaptable molecular tools for studying biological systems. Specifically, their enduring photoluminescence, precise emission spectra, and significant Stokes shifts allow for experiments not achievable with organic fluorophores or fluorescent proteins. Moreover, the capacity of these metal ions for luminescence resonance energy transfer and photon upconversion extends the potential applications of lanthanide probes even further. In this research, a new [Nd(NTA)2·H_2O]$^{3-}$ complex was synthesized and its optical properties were assessed using practical characterization techniques such as UV–Vis absorption, photoluminescence, and FTIR. It was discovered that when the sample was excited by a 357 nm wavelength, it emitted a strong line at 1076 nm with a full-width at half maximum (FWHM) of 10 nm, a phenomenon not previously documented. The Judd-Ofelt theory and its intensity parameters were utilized in a theoretical approach to determine the fluorescence branching ratio and the radiative lifetime of the [Nd(NTA)2·H_2O]$^{3-}$ complex. The absorption and luminescence spectra were then analyzed accordingly. Experimental findings validated the potential applications of the prepared sample in bioimaging.

1. Introduction

The incomplete 4F level, which is covered by 5s and 5p electron configurations, is used to identify lanthanide elements, which tend to lose electrons. Due to the proper shielding of 4f electrons from their surroundings, these levels appear as parallel parabolas that can be found in Fig. 1a. Typically, all lanthanide elements exhibit the +3 valence state. The +4 and +2 valence states are stable mainly for the lanthanide ions with completely empty, half-full, or completely filled f shells. Similar to its trivalent cousins, the divalent lanthanide (Ln^{2+}) class also has [Xe]$4f^n$ electron configurations. The main difference lies in the $4f^{n-1}5\,d^1$ energy levels. In Ln^{2+} ions, the first $4f^{n-1}5\,d^1$ levels are lower in energy compared to those in Ln^{3+} ions, allowing the Laporte-allowed 5d states to be accessed with visible light [1]. Recent studies have highlighted the importance of $4f^{n-1}5\,d^1 \leftrightarrow 4f^n$ transitions due to their high intensities and short luminescence lifetimes [2,3]. Additionally, because the $4f^{n-1}5\,d^1$ levels have a strong interaction with the crystal field, it is possible to easily adjust the optical properties by altering the characteristics of the host compound [2,3]. However, Ln^{2+} ions are generally unstable in most host compounds [4], and comprehensive spectroscopic studies of several Ln^{2+} ions have only recently been conducted [5,6]. On the other hand, the improved non-invasive capabilities of near-infrared imaging, which spans wavelengths from 700 to 1700

* Corresponding author.
E-mail addresses: msghamsari@yahoo.com, msasani@aeoi.org.ir (M. Sasani Ghamsari).

https://doi.org/10.1016/j.heliyon.2024.e33139
Received 8 April 2024; Received in revised form 13 June 2024; Accepted 14 June 2024
Available online 15 June 2024

nm, have drawn a lot of attention from researchers in recent years [7,8]. Benefits include lower background interference, increased signal-to-noise ratio, deeper tissue penetration, and better imaging resolution. The main chemical challenge in NIR imaging is creating probes that absorb and/or emit in the NIR range while maintaining good biocompatibility, low toxicity, high brightness, and photostability. Inspired by the success of lanthanide coordination chemistry in visible optical imaging, such as with Eu^{3+} and Tb^{3+} ions, inorganic chemists have aimed to design NIR-emissive lanthanide coordination compounds for use in NIR bioimaging and biosensing [9,10]. NIR-emissive lanthanide (Ln) complexes offer the benefits of organic molecules, including compact size, high extinction coefficient, and adjustable excitation wavelength. Additionally, they exhibit appealing features due to coordination chemistry and metal-centered luminescence [11]. In biological imaging, lanthanide materials have a major impact on the sensitivity, resolution, and detection depth [12]. Because the rare earth ions are protected by the 5s and 5p orbitals, the environment has little effect on their fluorescence, which produces a consistent and crisp emission spectrum with a narrow peak. Resolution of fluorescence imaging is limited by the full width at half maximum (FWHM) of these ions, which is usually 10–20 nm, as opposed to 100 nm for transition metal ions and 25–40 nm for quantum dot materials. Owing to atomic transitions, the fluorescence emission from rare earth ions also shows a great resistance to photobleaching. Moreover, a customized emission band is made possible by doping with various rare earth ions; the fluorescence spectrum includes the ultraviolet, visible, and near-infrared ranges [12–14]. Consequently, lanthanide nanomaterials serve as highly effective non-invasive biological imaging contrast agents, enabling high-resolution and highly sensitive fluorescence imaging in living organisms [15]. To address the issue of narrower FWHM, several strategies have been effectively employed, including orthogonal excitation and/or detection of nanoprobes, Raman scattering under electronic pre-resonance conditions, and the use of multifilter techniques. The FWHM of current NIR–II–emitted nanoprobes ranges from approximately 70–100 nm for quantum dots (QDs), 15–30 nm for lanthanide downconversion nanoparticles (DCNPs) and lanthanide complexes, 35–150 nm for organic molecular probes, and 50–200 nm for carbon nanotubes (CNTs) [16]. Consequently, DCNPs and lanthanide complexes are the most suitable options for in vivo NIR-II multiplexed imaging, due to their flexible structural modification [17]. Therefore, lanthanide complexes are known as attractive luminescence materials due to their narrow emission band and long emission lifetime over a wide range of wavelengths (UV to NIR) [18,19]. Because of their water solubility, thermodynamic stability, absorption band at or above 405 nm, high brightness, and excited state lifetime in the micro- or millisecond range, the +4 Lanthanide (III) (Ln III) ions are widely used in the field of bioimaging. Soini et al. described the groundbreaking work on the use of Ln III in bioimaging [20]. In these applications, the raer earth ions must generally exhibit optical properties in an aqueous medium. In practice, this means that the ion must have strong near-IR (NIR) emission with a long lifetime to gate out the background fluorescence. Among rear earth ions, neodymium offers a significant advantage over europium and terbium due to its ability for near-infrared optical excitation and its emission in the second body window, which leads to a lower-lying emissive state in the NIR wavelength region. In addition, an aromatic chromophore can transfer the absorbed visible light energy into the Nd^{3+} ions and provide an NIR emission light source. In biological systems and bioimaging, the emission bands in near infrared are very influential because they have better penetration inside the scattering biological media. To this end, it is necessary to form a complex in which the metal ion is shielded from surrounding solvent molecules by the ligand skeleton [21,22]. Despite numerous developments in this area, there are still limitations in some types of bioimaging due to the lack of penetration of some light wavelengths into the tissues of the case. In order to overcome these limitations and further penetrate the light into the tissue, luminescence compounds must work in "biological windows" because of their partial transparency. In the past, most research on the activity of these compounds has been in the first biological window, which is in the range of 650 nm–950 nm. The luminescence compounds in this window behaved in two ways.

- ➢ They were excited in first biological window but radiated in another spectral region.
- ➢ They were excited both in the spectral region of first biological window and were emitted in that region.

Representatives of the first group include semiconductor quantum dots (QDs), gold nanorods, and rare earth elements that are doped in up-convert nanoparticles. The first group does not adequately solve the problem of penetration depth in tissues due to the

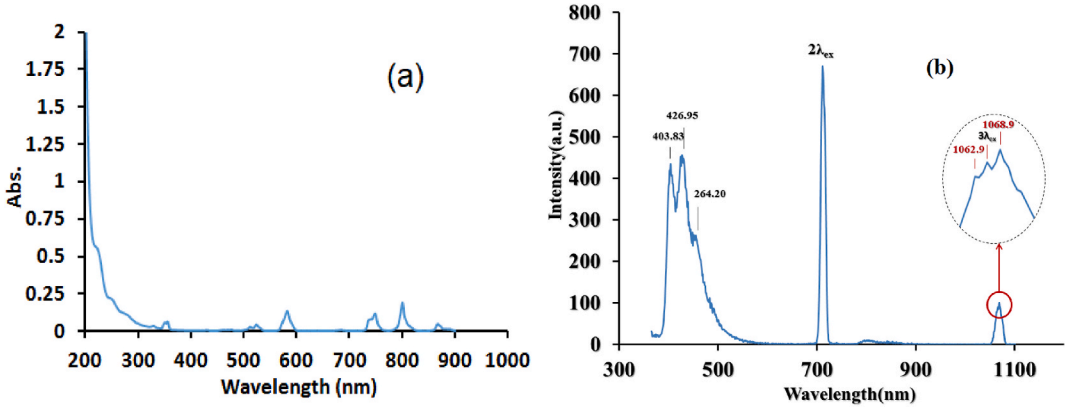

Fig. 1. (a) Absorption and (b) luminescence spectra of $Nd(NO_3)_3.6H_2O.4EDTA$ in methanol.

absorption and scattering of light [23]. The second group consists of compounds that are less absorbed by tissues than the first group and solve the problem of penetration depth for bioimaging. The second group is divided into two subgroups. The first subgroup consists of compounds that are involved in the process of multi-photon excitation, in which photons with higher energy are emitted after the absorption of lower-energy photons, such as $NaYF_4$ nanocrystals doped by some lanthanide ions of interest for luminescence such as Yb^{3+} or Tm^{3+}, or some nanoparticles such as Eu^{3+}:Y_2O_3, Er^{3+}:Y_2O_3 that are co-doped with Yb^{3+} or Tm^{3+}, etc. The second subgroup consists of compounds that can be involved in a single photon excitation process, in which the absorption of higher-energy photons (shorter wavelength) leads to emission with a longer wavelength than excitation photons, such as doping Nd^{3+} or Er^{3+} in nanocrystals. These processes can be divided into two types: quantum cutting and downshifting. In quantum cutting, a higher-energy photon is transformed into two lower-energy photons. In downshifting, a higher-energy photon is transformed into a longer wavelength, and excess energy is lost in the form of heat [23,24]. Researchers are currently focusing on luminescence compounds working in the second biological window in the 1000 nm–1400 nm band. This band, due to the longer wavelengths than the first biological window, has less light scattering, which therefore increases the penetration depth and improves the quality of sub-tissue images. By far, the best combination for bioimaging in the second biological window was carbon nanotubes, which have been used to anatomically image the deep-tissues of small animals such as mice. But it has serious drawbacks, including low quantum efficiency (less than 10 %). Among these complexes, some of them, such as Nd^{3+}-doped nanoparticles, attract more attention due to their phonon vibration energy, synthesis methods, special optical properties, and high quantum efficiency [25]. Hasegawa and Kitagawa [26] believed that if the luminescent lanthanide (III) complexes show narrow emission bands (full widths at half maximum (FWHM) < 10 nm in the visible region) based on 4f–4f transitions, they will be suitable for biological applications. In this study, we tried to control the radiationless transition processes, dipole-dipole non-radiative energy transfer processes, and perturbation of Nd^{3+} f orbitals in Nd^{3+} complexes contacting certain ligands and considering the effect of the crystal field to decrease the FWHM value ($\leq$10 nm). An innovative method was created and used for the first time in order to meet the mentioned goal.

2. Experimental studies

2.1. Materials

Various types of raw materials were used in this investigation and in the synthesis of the samples. Without undergoing additional purification, all raw ingredients were obtained from commercial vendors (Sigma Aldrich and Merch). The analytical reagent grade starting ingredients, which were acquired from Sigma Aldrich, included $Nd(NO_3)_3$.6H2O, nitrilotriacetic acid (NTA), diethylenetriaminepentaacetic acid (DTPA), dimethylsulfoxide (DMSO), triethylamine (Et_3N), ammonium hydroxide, and ethylenediaminetetraacetic acid (EDTA). From Merch, further materials were developed.

2.2. Methods

To prepare Nd^{3+} complexes, we have used two different approaches. In the first approach, the Nd^{3+} complex was synthesized using the purchased $Nd(NO_3)_3.6H_2O$. To prepare the first sample, an appropriate amount of neodymium nitrate was dissolved in 80 ml of methanol. Then ethylenediaminetetraacetic acid (EDTA) was added to the original solution and mixed for several hours by the magnetic stirrer. After a few hours, the solution was placed in an ultrasonic bath to achieve greater homogeneity. In the second approach, neodymium nitrate was prepared in our laboratory. To synthesize the neodymium nitrate, 3.364 gr of Nd_2O_3 was mixed with 20 ml of distilled water on a magnetic stirrer at a temperature of 60 °C, and 2.7 cc of nitric acid was added drop by drop to it until it gave us a stable purple color. After several hours, the solution was put in a vacuum oven, and it stayed at 65 °C for a day until it dried. After one day, we mix the obtained material with 5 cc of distilled water, put it in the oven again, and dry it. Then the obtained powder was dissolved in 5 cc of dimethyl sulfoxide solvent. To synthesize the novel complex of neodymium ions, we prepared a mixture of DMSO and triethylamine (Et_3N). Then, an appropriate amount of $Nd(NO_3)_3.5H_2O$ was added to the resulting solution at 40 °C. Finally, ammonium hydroxide was added to the solution and stirred again for 15–20 min at the same temperature.

2.3. Characterization and instruments

The materials' absorption spectra were recorded using the Varian Co. 500 UV–vis spectrophotometer. A PANalytical (XPertPRo MPD) diffractometer was used to apply the X-ray diffraction pattern. A Bruker Alpha II FTIR spectrometer is used to plot the Fourier transform infrared (FTIR) spectrum, which analyzes the structure and purity of the material as well as the variations in chemical bonds. Lastly, the Gilden Photonics PL spectrometer was used to conduct photoluminescence spectroscopy in order to ascertain the optical characteristics of the samples.

3. Results and discussion

The absorption and emission spectra of the first sample are shown in Fig. 1. Fig. 1a shows the absorption of the prepared sample. The absorption peak intensity as a function of the wavelength is not too high. As can be seen in Fig. 1b, the luminescence spectrum of the prepared solution includes several peaks. The highest peak is actually the 2λ peak of the device, which is twice the excitation wavelength of 357 nm. The emission peak located near the 1065 nm wavelength is due to the sample and has a good peak width and relatively good intensity, which must be improved.

In this range, several peaks have appeared together, one of which is definitely 3λ of the device, or three times the excitation wavelength. The middle peak has a wavelength of 1065, which is three times the excitation wavelength. But the two side peaks of 3λ, namely 1068.9 and 1062.9, are peaks related to the sample itself. To enhance the emission intensity, simple ligands such as nitrilotriacetic acid (NTA) were used instead of EDTA. The absorption and emission spectra of the prepared sample in the presence of NTA are shown in Fig. 2. The absorption peak intensity as a function of the wavelength for this sample is too high. Also, the emission peaks have a higher intensity.

As it has been pointed out by Beeby and Faulkner [27], simple ligands such as nitrilotriacetic acid (NTA) lead to a small increase in lifetime, while the lifetime increases on moving to the six-coordinate ligand EDTA and again on complexation with DTPA, which is potentially 8-coordinate. To eliminate the effects caused by the solvent bonds or the quenching effect and increase the peak intensity of the emission line, it was decided to prepare a sample of neodymium nitrate powder with fewer water molecules. In this regard, many studies and laboratory work were done. The X-ray diffraction spectrum of the product obtained at this stage is shown in Fig. 3. As mentioned in our previous article [28], nanostructured lanthanide nitride compounds with five water molecules exhibit unique intricacies. Accurately identifying the crystallographic planes of the peaks in the X-ray diffraction spectrum of these compounds necessitates the utilization of specialized software and a substantial level of expertise in plane identification [29]. Consequently, we refrained from indexing these peaks to prevent any potential inaccuracies. Fig. 4 shows the FTIR spectrum of the synthesized Nd $(NO_3)_3.5H_2O$ dissolved in methanol. In the FTIR spectrum, the wave number of 1043 is due to the C–O stretch bonds.

And the wave numbers of 1350 cm^{-1} to 1380 cm^{-1} indicate the presence of vibration groups N–O and NO^{3-} in the composition, which is caused by the nitric acid used in the synthesis of the substance. The wave numbers of 1470 and 1637, respectively, represent the bonds of C–C and –NH_2 in the composition, and we also have the bond of C═N in the wave number of 2055 cm^{-1}. Strong absorption in the range of 500 cm^{-1} to 800 cm^{-1} indicates the presence of π-NO_3 vibrational bonds and confirms the existence of nitrate and possibly Nd oxide compounds [30,31]. To compare the optical properties of the synthesized $Nd(NO_3)_3.5H_2O$, NTA was used as a ligand. Absorption and luminescence spectra of the synthesized $[Nd(NTA)2{\cdot}H_2O]^{3-}$in dimethyl sulfoxide solvent (sample M22) are shown in Fig. 5 a,b.

Apparently, the photoluminescence spectrum has only one peak at 1080 nm in the range of 1000–1100 nm (Fig. 5b). However, the peak consists of three peaks that can be considered at 1078, 1080, and 1082 nm. These peaks are related to neodymium, and with three times 357, which is equivalent to 1071, they are related to the device itself. However, the intensity of its 1080 peak is not too high. Previously, Bukietynska and Mondry [32] reported the spectroscopic properties of Ho^{3+}-NTA and Er^{3+}-NTA systems with different M:L ratios within a broad pH range. They analyzed the oscillator strength values of the 'hypersensitive' transitions and of the Judd-Ofelt intensity parameters τλ and found the type of bonding of the Ln^{3+}-NTA species occurring in solution. They found that in the ratio of 1:2, each ligand molecule is coordinated by three oxygen and one nitrogen atom [32]. They concluded that if the coordination number of the Ho^{3+} is 8, no water molecule is preserved in the first-coordination sphere of the lanthanide ion. If the coordination number of the Ho^{3+} is 9, only one water molecule can be preserved. Such a complex hydrolyzes with difficulty because the water molecule in the lanthanide first-coordination sphere is more easily substituted by the OH group. For the L:M ratio higher than 1:2, no distinct spectral differences were observed, and therefore, under these conditions, no higher complexes should exist in the system considered [32]. It has been demonstrated that the O–H bond is very harmful for the optical properties of Nd^{3+} complexes [33,34]. Using the energy gap theory, Stein and Würzberg have shown that the presence of C–H or O–H bonds in the vicinity of Nd^{3+} leads to effective radiationless transitions [35]. They concluded that the vibrational excitation of these bonds leads to a reduction in emission quantum yields [35]. To suppress the effect of such vibrational excitation, different strategies like the use of deuterated solvents with low vibrational frequencies, deuteration of C–H and O–H bonds, or replacement of C–H bonds with C–F bonds in ligating molecules have been used [36,37]. To enhance the intensity of light emission by the sample M22, it was mixed with the novel $[Nd(HCO_2)_3.0.2H_2O]$ complex of (M25). Klink et al., the presence of Et_3N as a base leads to the formation of the complexes readily upon addition of the lanthanide nitrate salts to the ligands [38]. In addition, Lee and co-workers [39], reported that the degradation of DMSO during its UV/H_2O_2 treatment was classified into two major pathways. According to their study, the kinetic model proposed in this study for the degradation of DMSO by –OH in the UV/H_2O_2 process was able to successfully predict the patterns of concentration time-profiles of all

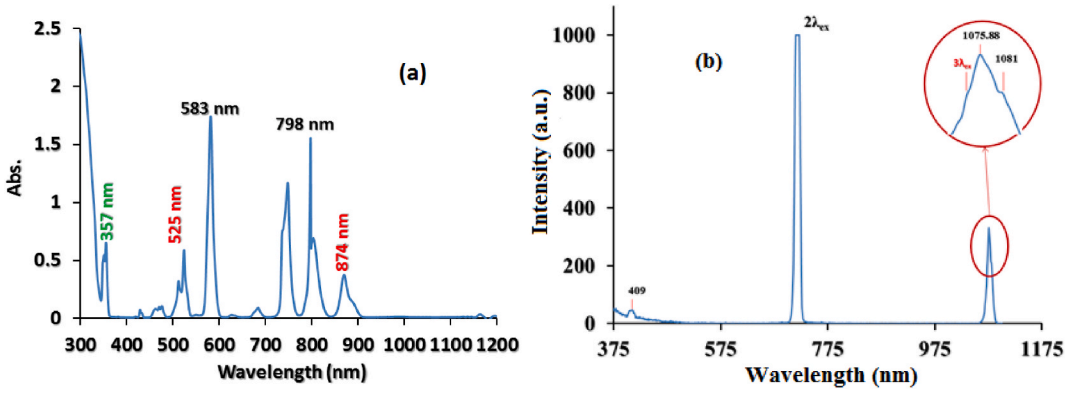

Fig. 2. (a) Absorption and (b) luminescence spectra of $[Nd(NTA)2{\cdot}H_2O]^{3-}$in DMSO.

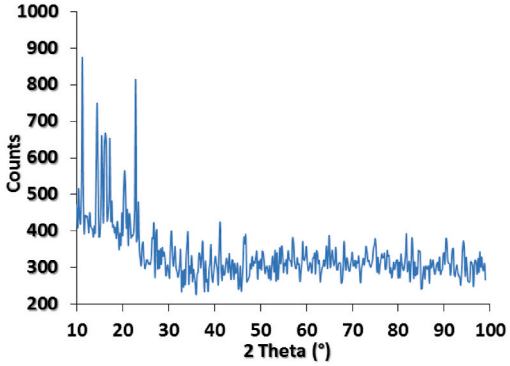

Fig. 3. XRD diffraction pattern of the synthesized $Nd(NO_3)_3.5H_2O$ according to JCPDS code 00-022-0738.

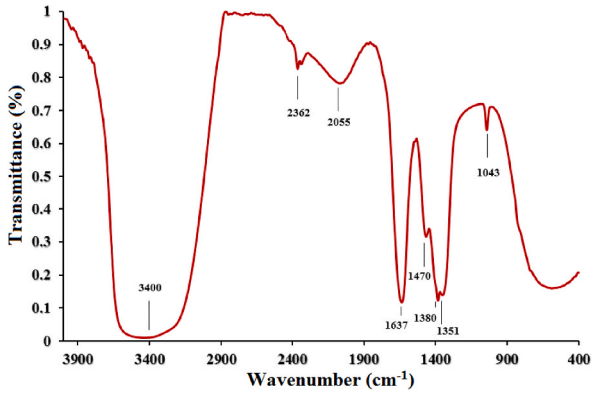

Fig. 4. FTIR spectrum of the synthesized $Nd(NO_3)_3.5H_2O$ dissolved in methanol.

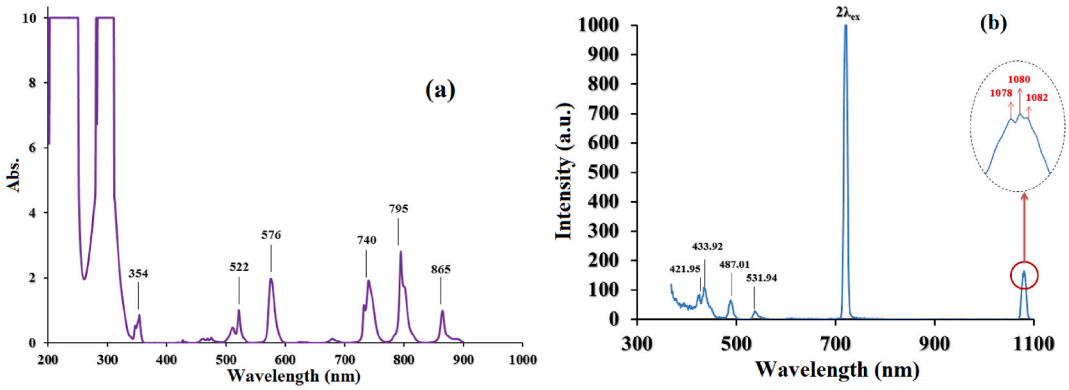

Fig. 5. (a) Absorption and (b) luminescnce spectra of the synthesized $[Nd(NTA)2{\cdot}H_2O]^{3-}$in DMSO.

components during the UV/H_2O_2 treatment of DMSO. Therefore, we believe that the presence of the ammonium hydroxide in the solution provides other carbon constituent of DMSO was relatively easily mineralized through the formation of formate (HCO_2^-) as non-sulfur-containing intermediates and $Nd(HCO_2)_3$. Fig. 6 shows the absorption spectrum of the novel complex of Nd^{3+}. Then, the effect of a novel complex of neodymium ions on the optical properties of sample M22 was evaluated using photoluminescence spectroscopy. For this purpose, small amounts of the novel complex of Nd^{3+} were mixed with sample M22, and then the emission characteristics of the mixed samples (M25+M22) were investigated.

The photoluminescence spectra of the mixed samples (M25+M22) in dimethyl sulfoxide solvent are shown in Fig. 7. The recorded peaks in the photoluminescence spectrum of the synthesized sample are in the range of 1000–1100 nm. Among these peaks, the only one at 1076 nm is the one related to neodymium ions. It has been found that the excited sample at 357 nm wavelength has an emission line at 1076 nm wavelength with 10 nm in full-width at half maximum (FWHM) that has not previously been reported. To make sure

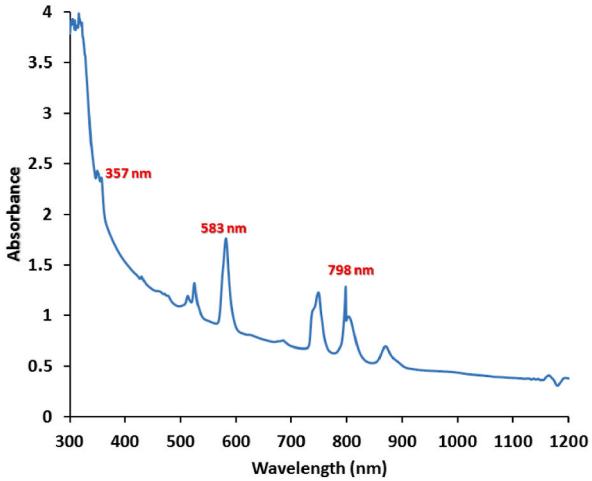

Fig. 6. Absorption spectrum of the novel complex of neodymium ions.

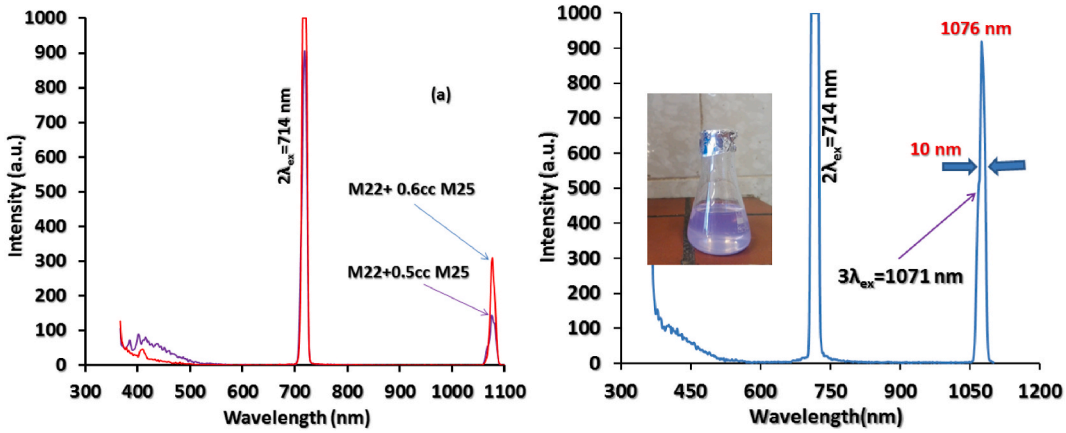

Fig. 7. The photoluminescence spectra of the sample M22 mixed with different concentration of the novel complex of Nd^{3+}.

that the mixed samples (M25+M22), the spontaneous transition probability, the fluorescence branching ratio, and the radiative lifetime of the Nd^{3+} complex are determined, Using Judd-Ofelt theory and its intensity parameters, these parameters of the Nd^{3+} complex were calculated and then analyzed in terms of its absorption and luminescence spectra.

There are three possible sources of lanthanide ion luminescence: charge-transfer transitions (LMCT and MLCT), intraconfigurational 4f-4f transitions, and interconfigurational $4f^n \rightarrow 4f^n5d1$ transitions. Previously, Misra and Sommerer [40] figured out that the f-f transition spectra of Nd(III) perchlorate in DMF, DMSO, and mixed H_2O-DMSO gave two bands, and their relative intensities were attributed to the different ratios of nona- and octacoordinated Nd(II1) solvated species where $[Nd(DMF)_9]^{3+}/[Nd(DMSO)_9]^{3+}$were the major species and $[Nd(DMF)_8]^{3+}/[Nd(DMSO)_8]^{3+}$were the minor species. Although the ratios of nona- and octacoordinated Nd(III) solvated species may vary in our study, the luminescence intensity increased by 300 % for the mixed sample. This enhancement cannot be attributed to intraconfigurational 4f-4f transitions or interconfigurational $4f^n \rightarrow 4f^n5d1$ transitions. It appears that the charge-transfer transitions (both LMCT and MLCT) play a crucial role in determining the emission light characteristics of the sample. When a UV photon is absorbed, it causes an electron to transition from the $^1S_0$ ground singlet state to the $^1S_1^*$ excited vibrational state of the organic environment. This is followed by relaxation to the lowest $^1S_1$ excited vibrational state, with the relaxation rate indicated as γ_{ic}^{nr}. Subsequently, there are two possible relaxation pathways from $^1S_1 \rightarrow S_0$: fluorescence with a transition rate of approximately $\gamma_f^r \sim 10^8\ s^{-1}$ [41], and a non-radiative process with γ_f^{nr} rate. Direct energy transfer from the singlet level of the ligand environment to the ion levels is also possible; the corresponding rate is γ_s^{et}. Additionally, intersystem crossing can give rise to the transitions from $^1S_1$ singlet level to T triplet level at γ_{isc}^{nr} rate. Relaxation from the triplet state (T) to the singlet state ($^1S_0$) is generally forbidden by selection rules because it requires a spin flip. However, in lanthanide complexes, these selection rules are partially relaxed due to spin-orbit interaction [41]. When different ligands are mixed, another mechanism called the antenna effect is introduced into the energy transfer process. Kotova et al. [42], previously studied the influence of different ligands on the photoluminescence characteristics of Eu complexes. They reported that changes in the absorption, fluorescence, and Eu(III)-centered emission spectra observed upon titrating

Eu(III) with 1(S) and 1(R) were identical for both enantiomers. The changes seen upon titrating 1(S) are shown in Fig. 8. According to their description, the absorption spectrum of 1(S) shows two main maxima at 222 and 270 nm (Fig. 8A). The alterations observed when titrating 1(S) are depicted in Fig. 8. As described, the absorption spectrum of 1(S) exhibits two primary peaks at 222 and 270 nm (Fig. 8A). Here, they first saw an increase in absorbance when the concentration of $Eu(CF_3SO_3)_3$ was raised. According to their experimental findings, the emission intensity rose as the concentration of $Eu(CF_3SO_3)_3$ increased, as we did in our experiment (Fig. 8).

The qualitative calculations of the intensities of the 4f–4f electronic transitions of these complexes have been developed by Judd and Ofelt. According to Judd-Ofelt (J-O) theory, the spectral intensities are expressed in terms of oscillator strengths. The experimental form of oscillator strength that is calculated from the area of the absorption band under the Gaussian curve is:

$$f_{\exp} = \left(2303\frac{mc^2}{N_A \pi e_2}\right)\int \varepsilon(\nu)d\nu \tag{1}$$

where N_A is the Avogadro number, m is electron mass, c is the light velocity, e is the electron charge and ε (ν) is the molar absorption coefficient. This equation reduces to:

$$f_{\exp} = 4.32 \times 10^{-9}\int \varepsilon(\nu)d\nu \tag{2}$$

The molar absorption coefficient ($\varepsilon(\nu)$) at a given energy is evaluated from the Beer–Lambert Law:

$$\varepsilon(\nu) = \frac{1}{cl}\log\left(\frac{I_0}{I}\right) \tag{3}$$

where c is the concentration of ion (mol%), l is the thickness of the glass (cm) and log (I_0/I) is the absorptivity (A) or the optical density (OD). The expression for calculated oscillator strength of a transition of average frequency (ν) from a level (Ψ_J) to a level ($\Psi' j'$) is given by:

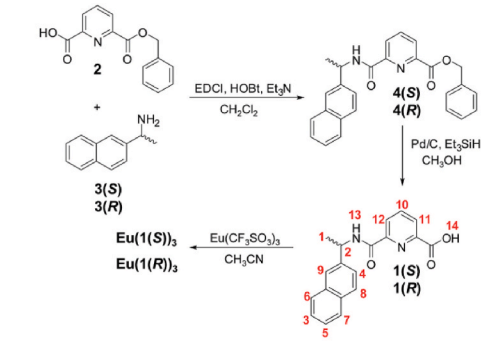

Scheme 1 Synthesis of the ligands 1(*S*) and 1(*R*), and their corresponding complexes $Eu(1(S))_3$ and $Eu(1(R))_3$ synthesized under microwave irradiation.

Fig. 8. The changes in the (A) absorption, (B) fluorescence and (C) Eu(III)-centered emission spectra of 1(S) ($c = 1 \times 10^5$ M) upon addition of Eu $(CF_3SO_3)_3$ in CH_3CN (25 C, 0.05 M $(C_2H_5)_4NCl$) [42].

$$f_{cal}\left(\Psi_j, \Psi'_{j'}\right) = \frac{8\pi^2 m\upsilon}{3h(2J+l)e^2}\left[\frac{\left(n_d^2+2\right)^2}{9n_d}\right]S_{ed} + n_d^3 d_{md} \tag{4}$$

where h is Planck constant, n_d is the refractive index of the medium at the sodium D line, S_{ed} is the electric dipole line strength and S_{md} is the line strength for the magnetic dipole to calculate absorption and radiative properties of emission transitions that could be obtained by the expressions

$$S_{ed} = e^2 \sum\nolimits_2^6 \Omega_\lambda \left(\Psi_j \left\| U^\lambda \right\| \Psi'_{j'}\right)^2 \tag{5}$$

$$S_{md}(\Psi j, \Psi' j') = \frac{e^2 h^2}{16c^2 m^2 \pi^2}\left(\Psi_j \| L + 2s \| \Psi'_{j'}\right)^2 \tag{6}$$

in which the unit tensor operators are shown by $\left\|U^\lambda\right\|^2$ of rank $\lambda = 2,4,6$ and Ω_λ are J-O parameters which determined with least squares fitting method [27,30,31]. The root mean square between f_{exp} and f_{cal} that indicates the J-O theory validity is:

$$\sigma_{rms} = \left[\frac{\sum\left(f_{\exp} - f_{cal}\right)^2}{\varepsilon - 3}\right]^{1/2} \tag{7}$$

where ε is the number of transitions concerned in the J-O parameter calculation [43–46]. The magnetic dipole line strengths have not been considered since the sharp lines arising due to f-f transitions are essentially electric dipole in nature. For emission (or luminescence) spectra, the spontaneous emission coefficient (also called transition probability for spontaneous emission or the Einstein coefficient for spontaneous emission (A $\left(\Psi_j, \Psi'_{j'}\right)$) can be written as:

$$A(\Psi j, \Psi' j') = \frac{64\pi^4 \upsilon^3}{3h(2J+l)}\left[\frac{n_d\left(n_d^2+2\right)^2}{9}S_{ed} + n_d^3 S_{md}\right] \tag{8}$$

Because an excited state Ψ_j is relaxed to several lower-lying states Ψ'_j the radiative branching ratio β_R is defined as:

$$\beta_R\left(\Psi_j, \Psi'_{j'}\right) = \frac{A\left(\Psi_j, \Psi'_{j'}\right)}{\sum_{\Psi' j'} A\left(\Psi_j, \Psi'_{j'}\right)} \tag{9}$$

where the factor in the denominator is the total radiative transition probability. The branching ratios can be used to predict the relative intensities of all emission lines originating from a given excited state. The experimental branching ratio can be found from the relative areas of the emission lines. Once all emission probabilities that depopulate an initial level of $2s+1L_j$ have been calculated, they can be used to determine how fast that level is depopulated. This rate is given by the radiative lifetime $\tau_R\left(\Psi_j\right)$ is given by:

$$\tau_R\left(\Psi_j\right) = \frac{1}{\sum_{\Psi' j'} A\left(\Psi_j, \Psi'_{j'}\right)} \tag{10}$$

stronger emission probabilities and more transitions from a level lead to faster decay and shorter lifetimes. The stimulated emission cross-section $\left(\sigma_p^E\ \mathrm{cm}^2\right)$ for all emission transitions have been computed from the formula:

$$\sigma_{em} = \frac{\lambda^4 A\left(\Psi_j, \Psi'_{j'}\right)}{8\pi c n^2} \times \frac{I(\lambda)}{\int I(\lambda) d\lambda} \tag{11}$$

where $I(\lambda)$ is the emission spectrum and is the index of refraction at wavelength λ [47,48]. Fig. 5a presents the absorption spectrum of the synthesized $Nd(NO_3)_3.5H_2O.4NTA$ in dimethyl sulfoxide solvent (sample M22). From this spectrum, experimental oscillator strengths have been calculated. Further J-O intensity parameters, Ω_λ, were calculated using the fitting approximation of the experimental oscillator strengths to the calculated oscillator strengths with respect to their electric dipole contributions. Also, spectroscopic quality factor $\frac{\Omega_4}{\Omega_6}$ was determined. The accuracy of fitting can be determined by the low ratio, which means that the lower square deviation, δ_{rms}, must be obtained as shown in Table 1. For the transition $4I_{9/2}$ to ($4G_{5/2}$, $2G_{7/2}$), 585 nm, the oscillator strength is very high when it is compared with others. Thus, it is known as a hypersensitive transition (HST). So this transition, because of its hypersensitivity, shows the maximum intensity in the absorption spectra. Based on J-O intensity parameters, the spontaneous transition probability A, fluorescence branching ratio β, and radiative lifetime τ_R were calculated and listed in Table 2. According to Fig. 4, the intensity of the spectra at 1076 nm was increased compared to Fig. 3b, and its FWHM was also decreased to 10 nm.

Table 1
The values of experimental and calculated oscillator strengths, the root mean square between them and J-O parameters of the prepared mixed sample.

Absorption transition $4I_{9/2}$ to	Wavelength (nm)	f_{exp} ($\times 10^{-6}$)	f_{cal} ($\times 10^{-6}$)
$2P_{1/2}$, $2D_{5/2}$	433	0.21	0.096
$2K_{15/2}$, $4G_{9/2}(2D, 2P)_{3/2}$, $2G_{91/2}$	476	1.41	1.15
$2k_{13/2}$, $4G_{7/2}$, $4G_{9/2}$	525	1.99	1.54
$4G_{5/2}$, $2G_{7/2}$	582	20.84	19.56
$4F_{9/2}$	681	0.42	0.28
$4F_{7/2}$,$4S_{3/2}$	746	7.64	6.88
$4F_{5/2}$, $2H_{9/2}$	802	3.11	2.35
$4F_{3/2}$	874	3.89	3.06
$\boldsymbol{\Omega_2}\left(\times 10^{-20}\mathbf{cm}^2\right)$	2.212		
$\boldsymbol{\Omega_4}\left(\times 10^{-20}\mathbf{cm}^2\right)$	0.652		
$\boldsymbol{\Omega_6}\left(\times 10^{-20}\mathbf{cm}^2\right)$	0.769		
$\frac{\boldsymbol{\Omega_4}}{\boldsymbol{\Omega_6}}$	0.847		
δ_{rms} ($\times 10^{-6}$)	0.755		

Table 2
The determined values of spontaneous emission transition probability, branching ratio, emission cross section and radiative lifetime of the prepared mixed sample.

Emission from excited state $4F_{3/2}$ to	Wavelength (nm)	$\boldsymbol{A}\left(\boldsymbol{\Psi_J}, \boldsymbol{\Psi}_{\boldsymbol{\Psi}}^{\boldsymbol{J}}\right)$ (S^{-1})	$\tau_R(\Psi_j)$ (ms)	$\boldsymbol{\beta}_{\boldsymbol{R}}\left(\boldsymbol{\Psi_J}, \boldsymbol{\Psi}_{\boldsymbol{\Psi}}^{\boldsymbol{J}}\right)\%$	σ_{em} ($\times 10^{-20}$ cm^{-2})
$4I_{11/2}$	1076	147.4152	6.8	59.32	5.2743

4. Conclusions

A novel $[Nd(NTA)2{\cdot}H_2O]^{3-}$ complex was prepared with various compositions and special methods. Spectral properties were studied with the Judd-Ofelt theory. The intensity parameters, Ω_λ, and radiative properties of the emission levels of this complex were evaluated. The simulated emission cross sections were also calculated. Due to the heaviness of the $[Nd(NTA)2{\cdot}H_2O]^{3-}$ complex and the need for more energy to excite, or because of the absorption in visible and infrared wavelengths by adjacent elements of the complex, the excitation wavelength in the UV region provided a peak at approximately 1076 nm. The lower the FWHM value, the higher the radiative photon intensity and quantum efficiency have been achieved. Intensive characteristic Nd^{3+} luminescence observed for both complexes under UV optical excitation provides the evidence for the "antenna" effect. Based on the spectroscopic data, the electronic transitions in the complex were identified and the diagram of its energy levels was developed. The influence of the ligand environment of the Nd^{3+} ion on its luminescence was analyzed in terms of the Judd-Ofelt intensity parameters. The values of spontaneous emission transition probability, branching ratio, emission cross section and radiative lifetime of the prepared mixed sample were determined.

CRediT authorship contribution statement

M. Sasani Ghamsari: Writing – review & editing, Validation, Project administration, Investigation, Data curation, Conceptualization. **M.M. Arghavan:** Writing – original draft, Methodology, Data curation.

Declaration of competing interest

The authors declare that they have no known competing financial interests or personal relationships that could have appeared to influence the work reported in this paper.

References

[1] J.J. Schuyt, S.V. Chong, G.V.M. Williams, " Luminescence of isoelectronic lanthanide pairs (Ln^{2+}/Ln^{3+}): a relative compression factor for isoelectronic Ln $4f^n$ levels", J. Lumin. 264 (2023) 120171.
[2] L. Yang, J. Luo, L. Gao, B. Song, J. Tang, Inorganic lanthanide compounds with f d transition: from materials to electroluminescence devices, J. Phys. Chem. Lett. 13 (2022) 4365–4373.
[3] L. Wang, P. Fang, Z. Zhao, Y. Huang, Z. Liu, Z. Bian, Rare earth complexes with 5d 4f transition: new emitters in organic light-emitting diodes, J. Phys. Chem. Lett. 13 (2022) 2686–2694.
[4] M. Suta, C. Wickleder, Synthesis spectroscopic properties and applications of divalent lanthanides apart from Eu^{2+}, J. Lumin. 210 (2019) 210–238.
[5] M. Karbowiak, C. Rudowicz, Trends in Hamiltonian parameters determined by systematic analysis of f-d absorption spectra of divalent lanthanides in alkali-halides hosts and supported by first calculations of the Nd^{2+} electronic structure: I. $SrCl_2$:Ln^{2+}, J. Lumin. 199 (2018) 116–125.
[6] M. Karbowiak, K. Maciejewska, C. Rudowicz, Trends in Hamiltonian parameters determined by systematic analysis of f-d absorption spectra of divalent lanthanides in alkali-halides hosts: III. $CsSrBr_3$:Ln^{2+} (Ln = Nd, Sm, Eu, Tm, and Yb), J. Lumin. 215 (2019) 116622.

[7] Y. Wu, H. Cao, S. Yang, C. Liu, Z. Han, Progress of near-infrared-II fluorescence in precision diagnosis and treatment of colorectal cancer, Heliyon 9 (2023) e23209.

[8] K Sai ManognaB Deva Prasad RajuG Rajasekhara ReddyParashuram KallemMannur Ismail ShaikN John Sushma, Investigations on anticancer activity of Eu^{3+} doped hydroxyapatite nanocomposites against MCF7 and 4T1 breast cancer cell lines: a structural and luminescence perspective, Heliyon 10 (2024) e23209.

[9] Y. Ning, M. Zhu, J.-L. Zhang, Near-infrared (NIR) lanthanide molecular probes for bioimaging and biosensing, Coord. Chem. Rev. 399 (2019) 213028.

[10] A.J. Amoroso, S.J. Pope, Using lanthanide ions in molecular bioimaging, Chem. Soc. Rev. 44 (2015) 4723–4742.

[11] S.J. Butler, M. Delbianco, L. Lamarque, B.K. McMahon, E.R. Neil, R. Pal, D. Parker, J.W. Walton, J.M. Zwier, EuroTracker® dyes: design, synthesis, structure and photophysical properties of very bright europium complexes and their use in bioassays and cellular optical imaging, Dalton Trans. 44 (2015) 4791–4803.

[12] Q. Fan, C. Sun, B. Hu, Q. Wang, Recent advances of lanthanide nanomaterials in Tumor NIR fluorescence detection and treatment, Materials Today Bio 20 (2023) 100646.

[13] J.H.S.K. Monteiro, Recent advances in luminescence imaging of biological systems using lanthanide(III) luminescent complexes, Molecules 25 (9) (2020) 2089.

[14] G.Q. Jin, Y.Y. Ning, J.X. Geng, Z.F. Jiang, Y. Wang, J.L. Zhang, Joining the journey to near infrared (NIR) imaging: the emerging role of lanthanides in the designing of molecular probes, Inorg. Chem. Front. 7 (2) (2020) 289–299.

[15] H. Li, X. Wang, D.X. Huang, G.Y. Chen, Recent advances of lanthanide-doped upconversion nanoparticles for biological applications, Nanotechnology 31 (7) (2020) 072001.

[16] Y. Yang, Y. Xie, F. Zhang, Second near-infrared window fluorescence nanoprobes for deep-tissue in vivo multiplexed bioimaging, Adv. Drug Deliv. Rev. 193 (2023) 114697.

[17] X.Y. Zhu, X. Liu, H.X. Zhang, M.Y. Zhao, P. Pei, Y. Chen, Y.W. Yang, L.F. Lu, P. Yu, C.X. Sun, J. Ming, I.M. Abraham, A.M. El-Toni, A. Khan, F. Zhang, High-fidelity NIR-II multiplexed lifetime bioimaging with bright double interfaced lanthanide nanoparticles, Angew. Chem., Int. Ed. 60 (44) (2021) 23545–23551.

[18] Y. Hasegawa, Y. Kitagawa, T. Nakanishi, Effective photosensitized, electrosensitized, and mechanosensitized luminescence of lanthanide complexes, NPG Asia Mater. 10 (2018) 52–70.

[19] B.D. Rosal, U. Rocha, E.C. Ximendes, E.M. Rodriguez, D. Jaque, J.G. Sole, Nd^{+3} ions in nanomedicine: Perspective and applications, Opt. Mater. 3 (2016) 1–12.

[20] J.H.S.K. Monteiro, Recent advances in luminescence imaging of biological systems using lanthanide (III) luminescent complexes, Molecules 25 (2020) 1–34.

[21] U. Cho, J.K. Chen, lanthanide-based optical probes of biological systems, Cell Chem. Biol. 27 (8) (2020) 921–936.

[22] J.A. Cotruvo, the chemistry of lanthanides in bology: recent discoveries, emerging principles, and technological applications, ACS Cent. Sci. 5 (9) (2019) 1496–1506.

[23] U. Rocha, U.K. Komar, C. Jacinto, I. Villa, F. Sanz-Rodriguez, M.C. Iglesias dela Crus, A. Juarranz, E. Carrasco, F.C.J.M. Veggel, E. Bovero, J. Garcia Sole, D. Jaque, *Neodymium*-doped LaF_3 nanoparticles for fluorescence bioimaging in second biological window, Small 6 (2014) 1141–1154.

[24] X. Kang, Ch Li, Z. Cheng, P. Ma, Zh Hou, J. Lin, Lanthanide-doped hollow nanomaterials as theranostic agents, WIREs Nanomed. Nanobiotechnol. 6 (2014) 80–101.

[25] A.N. Carneiro Neto, E.E.S. Teotonio, G.F. de Sa, H.F. Brito, J. Legendziewicz, L.D. Carlos, M.C.F.C. Felinto, et al., " Modeling intramolecular energy transfer in lanthanide chelates: a critical review and recent advances", Handb. Phys. Chem. Rare Earths 56 (2019) 55–162.

[26] Y. Hasegawa, Y. Kitagawa, Thermo-sensitive luminescence of lanthanide complexes, clusters, coordination polymers and metal–organic frameworks with organic photosensitizers, J. Mater. Chem. C 7 (2019) 7494–7511.

[27] A. Beeby, S. Faulkner, Luminescence from neodymium (III) in solution, Chem. Phys. Lett. 266 (1997) 116–122.

[28] M.M. Arghavan, A.A. Sabouri-Dodaran, M. Sasani Ghamsari, Nanocrystalline Yttrium (III)-pentaaqua-trinitrate powders prepared using a facile route, Inorg. Chem. Commun. 156 (2023) 111196.

[29] Michael G.B. Drew, Mark R.StJ. Foreman, Michael J. Hudson, Karen F. Kennedy, Structural studies of lanthanide complexes with tetradentate nitrogen ligands, Inorg. Chim. Acta. 357 (2004) 4102–4112.

[30] A. Rout, K. Binnemans, Separation of rare earths from transition metals by liquid–liquid extraction from a molten salt hydrate to an ionic liquid phase, Dalton Trans. 43 (2014) 3186–3195.

[31] S. Zinatloo-Ajabshir, S. Mortazavi-Derazkola, M. Salavati-Niasari, Nd_2O_3 nanostructures: simple synthesis, characterization and its photocatalytic degradation of methylene blue, J. Mol. Liq. 234 (2017) 433–436.

[32] K. Bukietynska, A. Mondry, spectroscopy of heavy lanthanide complexes with NTA, Inorg. Chim. Acta. 130 (1987) 271–276.

[33] W.R. Dawson, J.L. Kropp, Measurement of fluorescence yields of europic ion upon excitation to selected levels, J. Opt. SOC. Am. 55 (1965) 822–828.

[34] J.L. Kropp, M.W. Windsor, Luminescence and energy transfer in solutions of rare-earth complexes. I. Enhancement of fluorescence by deuterium substitution, J. Chem. Phys. 42 (1965) 1599.

[35] G. Stein, E. Würzberg, Energy gap law in the solvent isotope effect on radiationless transitions of rare earth ions, J. Chem. Phys. 62 (1975) 208–213.

[36] M. Hasegawa, H. Ohmagari, H. Tanaka, K. Machida, Luminescence of lanthanide complexes: from fundamental to prospective approaches related to water- and molecular-stimuli, Journal of Photochemistry & Photobiology, C: Photochemistry Reviews 50 (2022) 100484.

[37] Y. Hasegawa, Y. Kitagawa, T. Nakanishi, Effective photosensitized, electrosensitized, and mechanosensitized luminescence of lanthanide complexes, NPG Asia Mater. 10 (2018) 52–70.

[38] S.I. Klink, L. Grave, D.N. Reinhoudt, F.C.J.M. van Veggel, M.H.V. Werts, F.A.J. Geurts, J.W. Hofstraat, A systematic study of the photophysical processes in polydentate triphenylene-functionalized Eu^{3+}, Tb^{3+}, Nd^{3+}, Yb^{3+}, and Er^{3+} complexes, J. Phys. Chem. A 104 (2000) 5457–5468.

[39] Y. Lee, C. Lee, J. Yoon, Kinetics and mechanisms of DMSO (dimethylsulfoxide) degradation by UV/H_2O_2 process, Water Res. 38 (2004) 2579–2588.

[40] S.N. Misra, S.O. Sommerer, absorption spectra of lanthanide complexes in solution, Appl. Spectrosc. Rev. 26 (1991) 151–202.

[41] D.A. Metlina, M.T. Metlin, S.A. Ambrozevich, I.V. Taydakov, K.A. Lyssenko, A.G. Vitukhnovsky, A.S. Selyukov, V.S. Krivobok, D.F. Aminev, A.S. Tobokhova, Luminescence and electronic structure of Nd^{3+} complex with pyrazolesubstituted 1,3-diketone and 1,10-phenanthroline, J. Lumin. 203 (2018) 546–553.

[42] O. Kotova, S. Blasco, B. Twamley, J. O'Brien, R.D. Peacock, J.A. Kitchen, M. Martınez-Calvoa, T. Gunnlaugsson, the application of chiroptical spectroscopy (circular dichroism) in quantifying binding events in lanthanide directed synthesis of chiral luminescent self-assembly structures, Chem. Sci. 6 (2015) 457–471.

[43] C.N.Y. Rajo, C.A. Reddy, S. Sailaja, H.J. Seo, B.S. Reddy, Judd-Ofel theory: optical absorption and NIR emission spectral studies of Nd^{+3}:CdO-Bi_2O_3-B_2O_3 glasses for laser applications, J. Mater. Sci. 47 (2012) 772–778.

[44] J.H. Choi, F.G. Shi, A.A. Margaryan, A. Margaryan, Spectral properties of Nd^{+3} ion in new fluorophosphates glasses: Judd-Ofelt intensity parameters, Proc. SPIE 4974 (2003) 121–127.

[45] B.M. Walsh, Judd-ofelt theory: principles and practices, Advances in Spectroscopy for Laser and Sensing (2006) 403–433.

[46] A.A. Kaminskii, G. Boulon, M. Bouncristiani, B.D. Bartolo, A. Kornienko, V. Mironov, Spectroscopy of new laser garnet $Lu_3Sc_2Ga_3O_{12}$:Nd^{+3}, Phys. Stat. Sol. 141 (1994) 471–494.

[47] Z.A.S. Mahraz, E.S. Sazali, M.R. Sahar, N.U. Amran, S.N.S. Yaacob, S.M. Aziz, S.Q. Mawlud, F.M. Noor, A.N. Harun, Spectroscopic investigations of near-infrared emission from Nd^{+3}- doped zinc-phosphate glasses: Judd-Ofelt evaluation, J. Non-Crystalline Solids 509 (2019) 106–114.

[48] Kh Nasser, V. Aseev, S. Ivanov, A. Ignatiev, N. Nikonorov, Optical, spectroscopic properties and Judd-Ofelt analysis of Nd^{+3}-doped photo-thermo-refractive glass, J. Lumin. 213 (2019) 255–262.